The role of Npt1 in regulating antifungal protein activity in filamentous fungi

Wang *et al.*

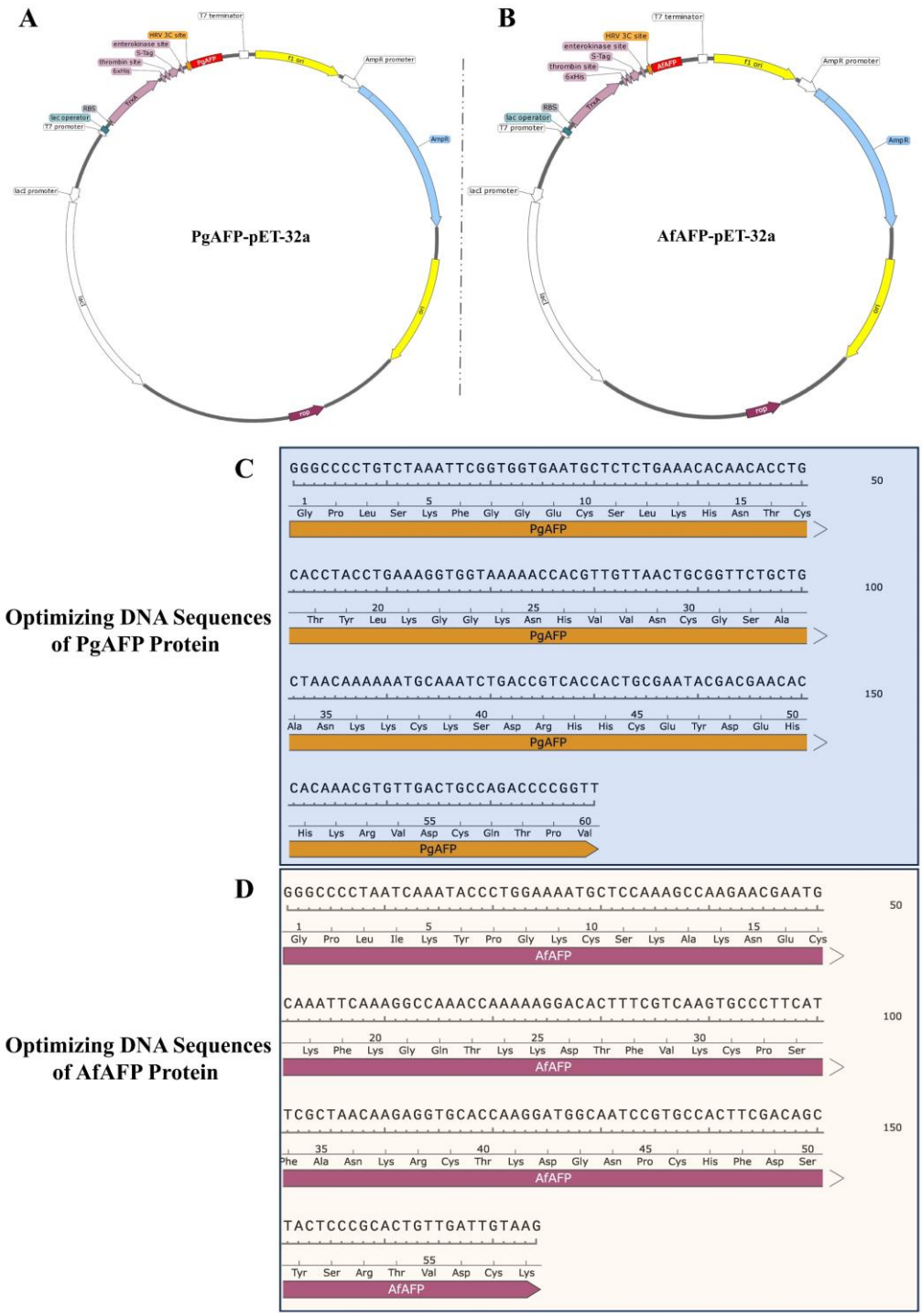

Supplementary Fig. 1. Plasmid construction and optimization of DNA sequences for recombinant expression of PgAFP and AfAFP proteins. (**A**, **B**) The plasmid profiles illustrate the insertion of genes encoding AfAFP and PgAFP. The pET-32a plasmid map, engineered for the recombinant expression of PgAFP and AfAFP, incorporated Trx and 6His tags. (**C**) Optimized DNA sequences for PgAFP protein. (**D**) Optimized DNA sequences for AfAFP protein.

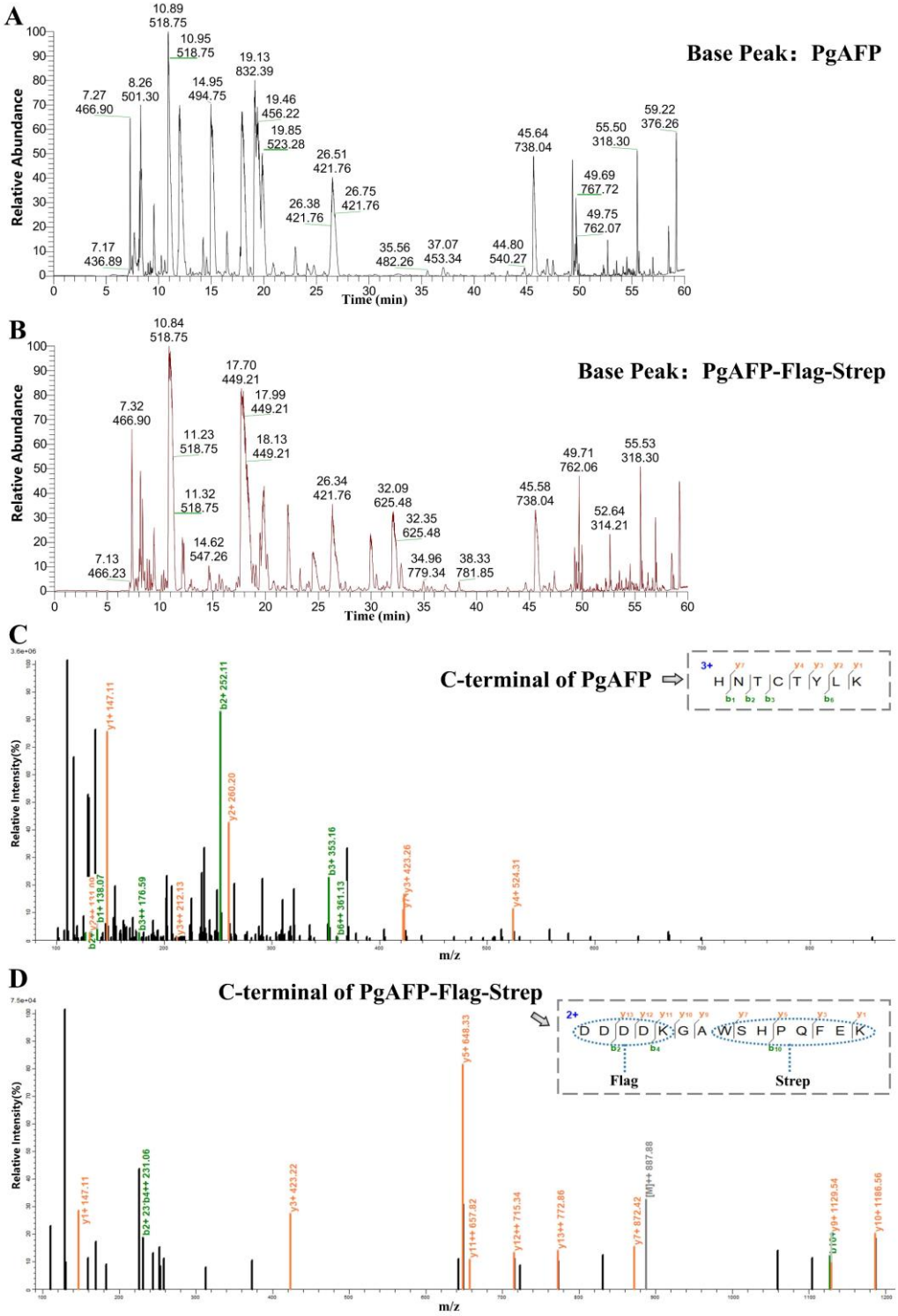

Supplementary Fig. 2. LC-MS/MS spectral analysis of recombinant PgAFP and its fusion proteins. (**A**, **B**) The LC-MS/MS spectral analysis verified the sequence integrity of the purified PgAFP and the PgAFP-Flag-Strep fusion protein. (**C**, **D**) The secondary mass spectrum analysis highlighted specific variations within the C-terminal regions of PgAFP and its Flag-Strep fusion counterpart.

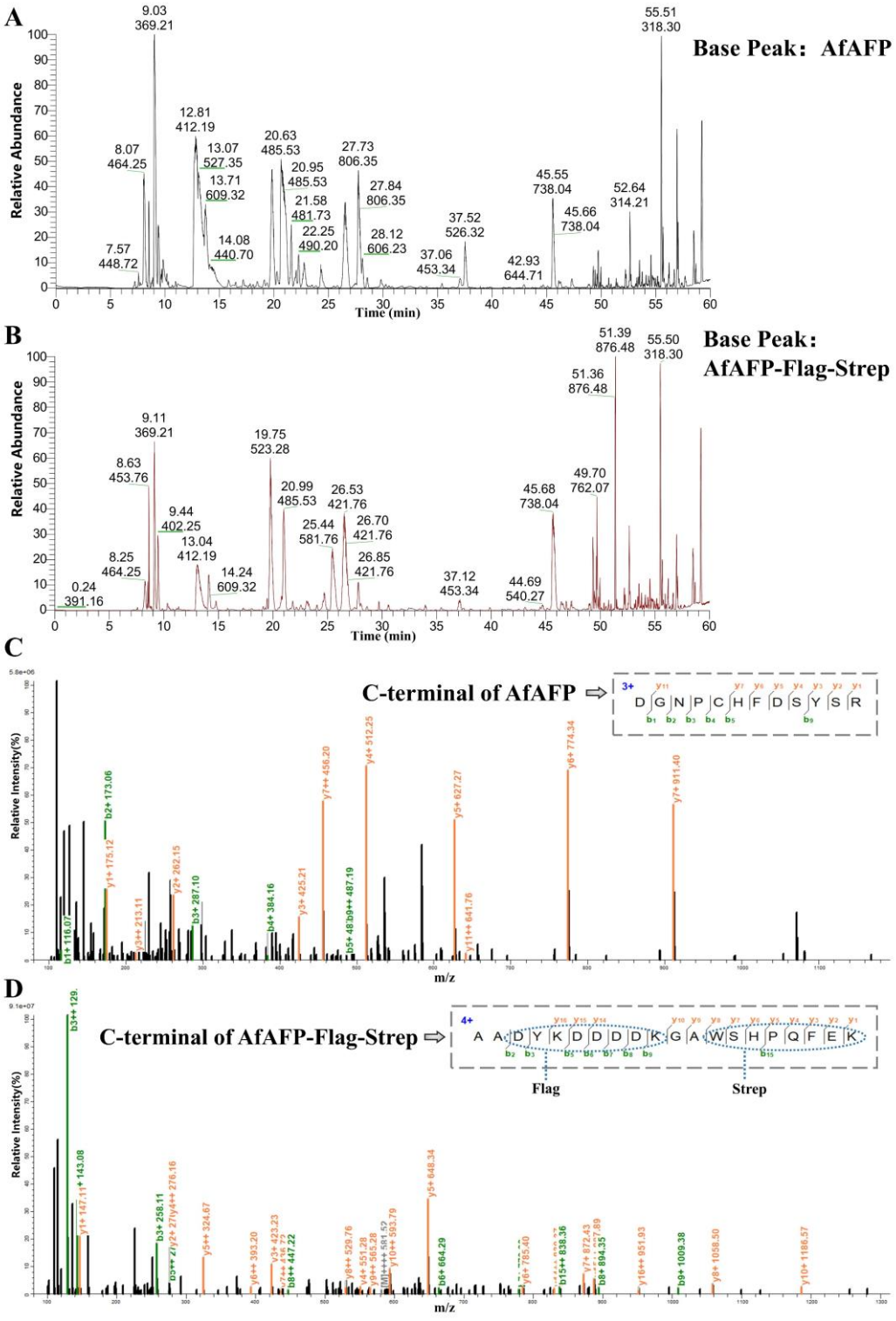

Supplementary Fig. 3. LC-MS/MS spectral analysis of recombinant AfAFP and its fusion variant. (**A**, **B**) The LC-MS/MS spectral analysis confirmed the sequence integrity of the purified AfAFP and the AfAFP-Flag-Strep fusion protein. (**C**, **D**) The secondary mass spectrum analysis revealed distinct disparities in the C-terminal regions of AfAFP and the AfAFP-Flag-Strep fusion protein.

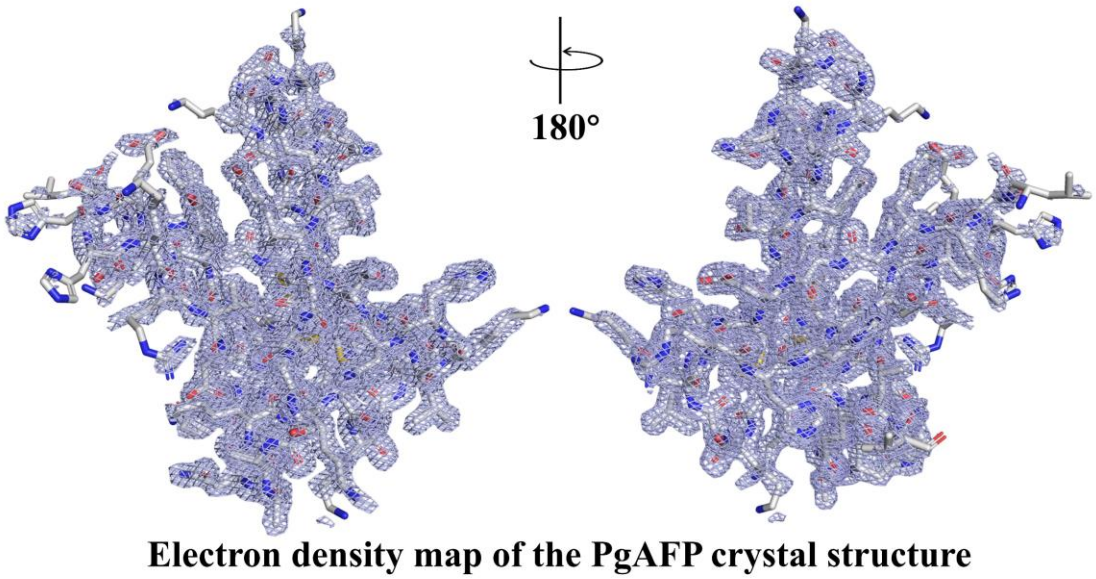

Supplementary Fig. 4. Electron density map of the PgAFP crystal structure. The electron density map is shown in light blue, contoured at 1σ for the 2Fo-Fc map.

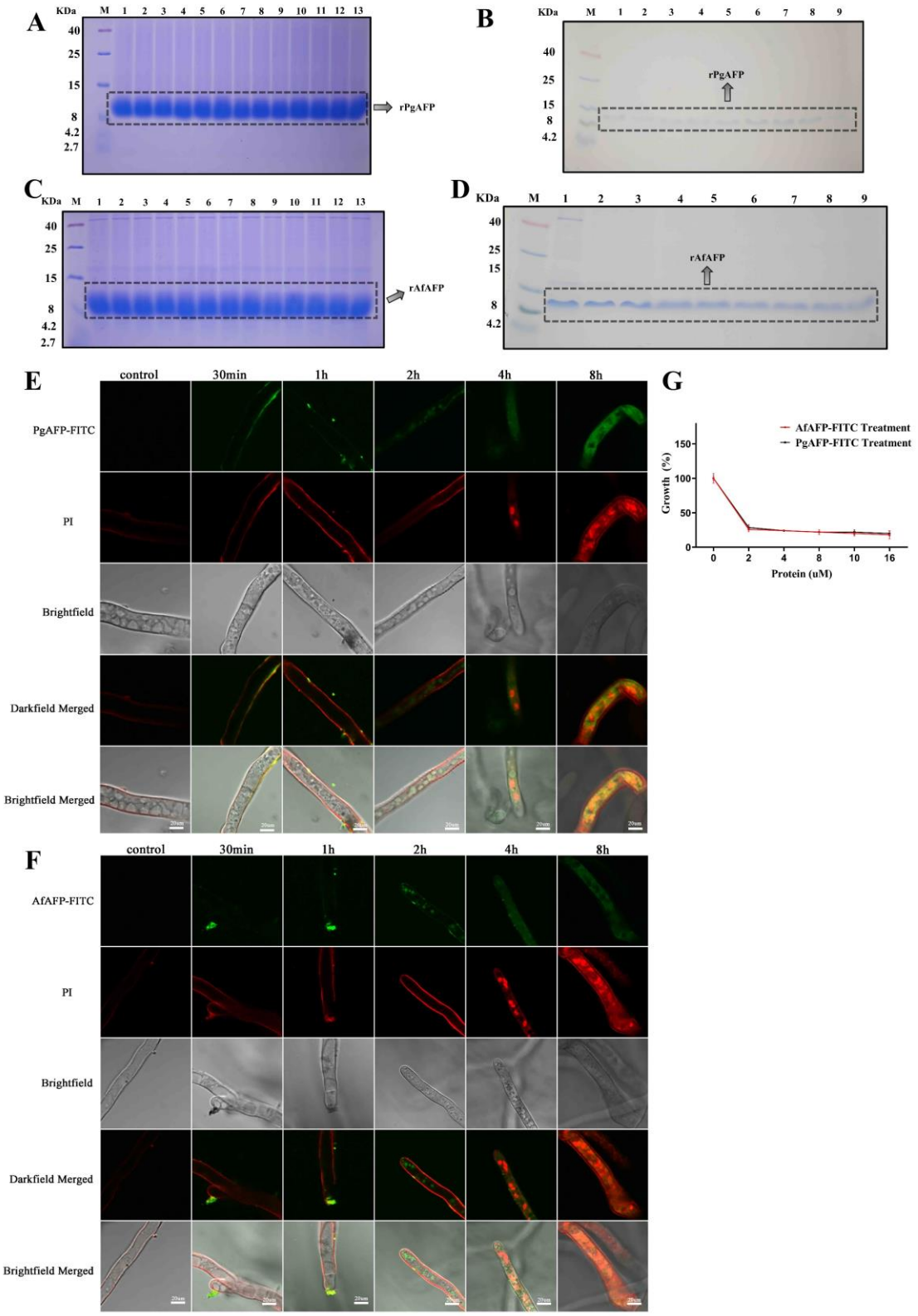

Supplementary Fig. 5. Temperature-dependent degradation and proteolytic stability of PgAFP and AfAFP and their intracellular localization in *A. flavus.* (**A**, **B**) PgAFP and AfAFP degradation test. Lane M: molecular weight marker; lane 1 is the untreated control; lanes 2–4 show the samples treated at 29 °C for 24, 48, and 72 h,

respectively; lanes 5–7 depict the 37 ℃ treatment for the same durations; lanes 8–10 show the 42 ℃ treatment for the same durations; and lanes 11–13 display the 50 ℃ treatment for the same durations. (**C**, **D**) PgAFP and AfAFP proteolytic test. Lane M: molecular weight marker; lane 1: control. Lanes 2 through 9 are treated with trypsin at varying weight-to-weight ratios, detailed as follows: lane 2 at 1:400, lane 3 at 1:300, lane 4 at 1:200, lane 5 at 1:100, lane 6 at 1:80, lane 7 at 1:60, lane 8 at 1:40, and lane 9 at 1:20. (**E**, **F**) Localization of AfAFP and PgAFP in *A. flavus*. The images detail the internalization process of FITC-labeled PgAFP and AfAFP into *A. flavus* cells. To assess the onset of fungal cell death, propidium iodide (PI) staining, which labels nucleic acids, was used. The results indicated that cell death commenced approximately 4 h post-treatment with either AFP, as evidenced by PI uptake. (**G**) Inhibitory effects of PgAFP–FITC and AfAFP–FITC on the *A. flavus* WT strain. The experiments described above included three biological replicates. Source data are provided as a Source Data file.

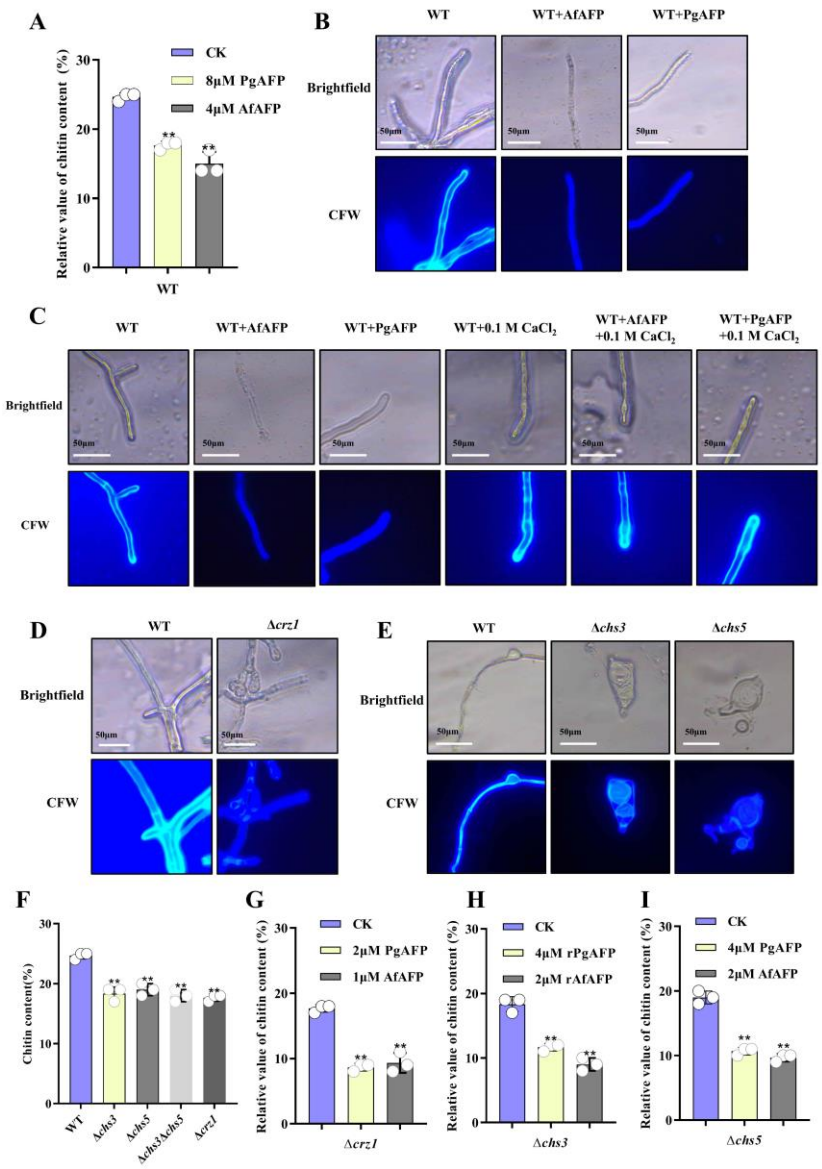

Supplementary Fig. 6. Assessing the influence of AFPs on mutant strains based on chitin content analysis. (**A**) The relative chitin content of the WT strain was measured following treatment with AFPs. (**B**, **C**) Fluorescence microscopy of *A. flavus* incubated with AfAFP or PgAFP in medium containing 0.1 M $CaCl_2$ for 12 h and stained with CFW. The exposure settings were identical for all samples. (**D**) WT and Δ*crz1* strains stained with CFW and visualized by fluorescence microscopy. Δ*crz1* is a mutant strain that lacks the calcineurin-responsive transcription factor Crz1. The exposure settings were identical for all strains. (**E**) Fluorescence microscopy of WT, Δ*chs3*, and Δ*chs5* strains stained with CFW, which revealed defects in chitin synthesis. The exposure settings were identical for all strains. (**F**) The relative chitin content was measured in the WT, Δ*crz1*, Δ*chs3*, and Δ*chs5* strains. (**G-I**) The relative chitin content of the Δ*crz1*, Δ*chs3*, and Δ*chs5* strains was assessed after adding AFPs. Source data are provided as a Source Data file.

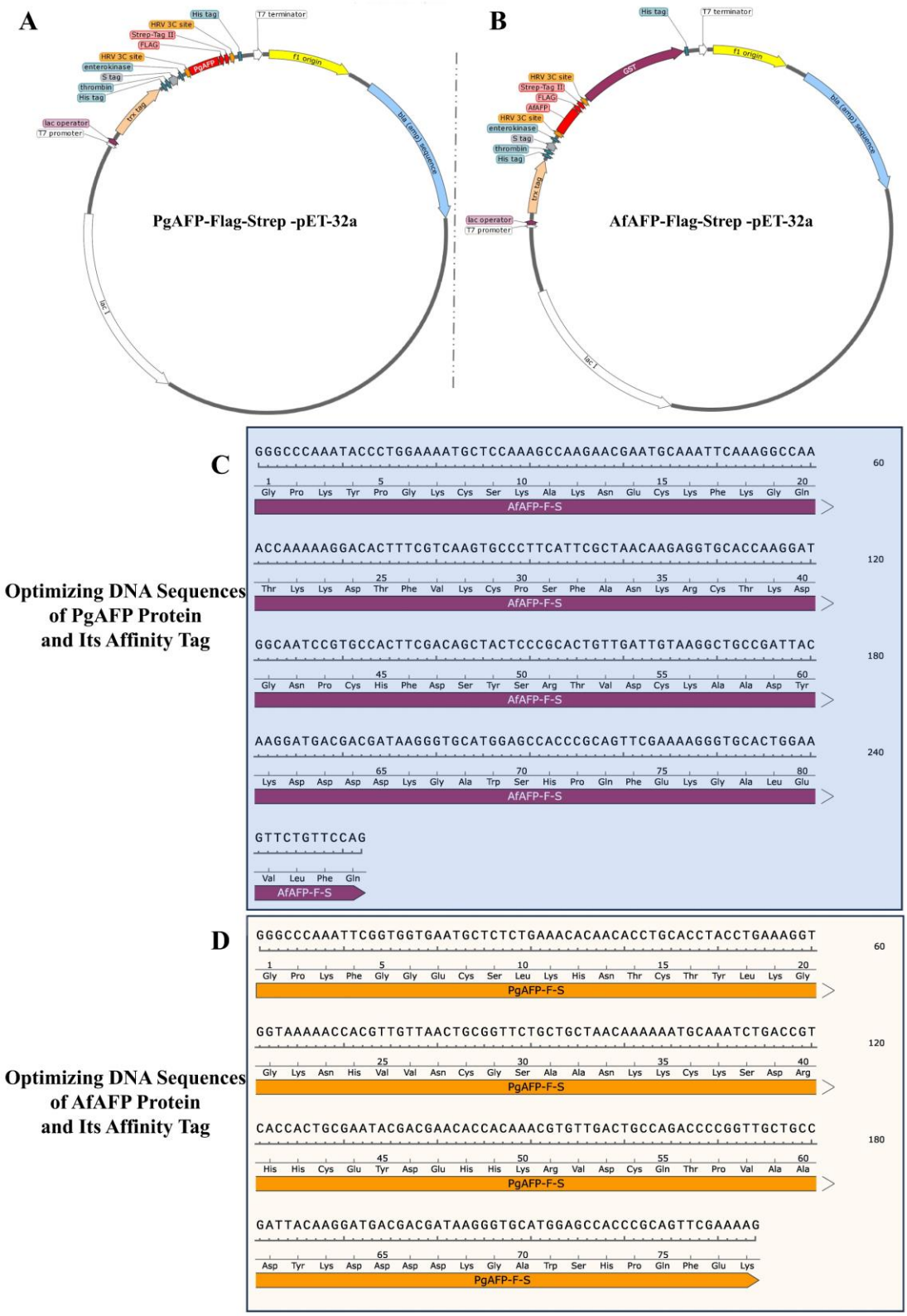

Supplementary Fig. 7. Strategic design and optimization of vector constructs for recombinant expression and purification of PgAFP and AfAFP proteins with affinity tags. (**A**) The pET-32a vector map used for recombinant expression of PgAFP with Trx, Flag, Strep, and 6His tags. Two PreScission protease sites were placed

strategically for tag removal during protein purification: one between the Trx and Flag tags, and another between PgAFP and the 6His tag. Post-purification, the PgAFP protein retained the Flag and Strep tags, while the other tags were cleaved via PreScission protease digestion. (**B**) The pET-32a vector map used for recombinant expression of AfAFP with Trx, Flag, Strep, GST, and 6His tags. There were two PreScission protease sites for removing the tags during protein purification: one between the Trx and Flag tags, and another between AfAFP and the GST tag. Post-purification, the AfAFP protein retained the Flag and Strep tags, while the other tags were designed for excision via PreScission protease digestion. (**C**) Optimizing DNA sequences of PgAFP protein and its affinity tag. (**D**) Optimizing DNA sequences of AfAFP protein and its affinity tag.

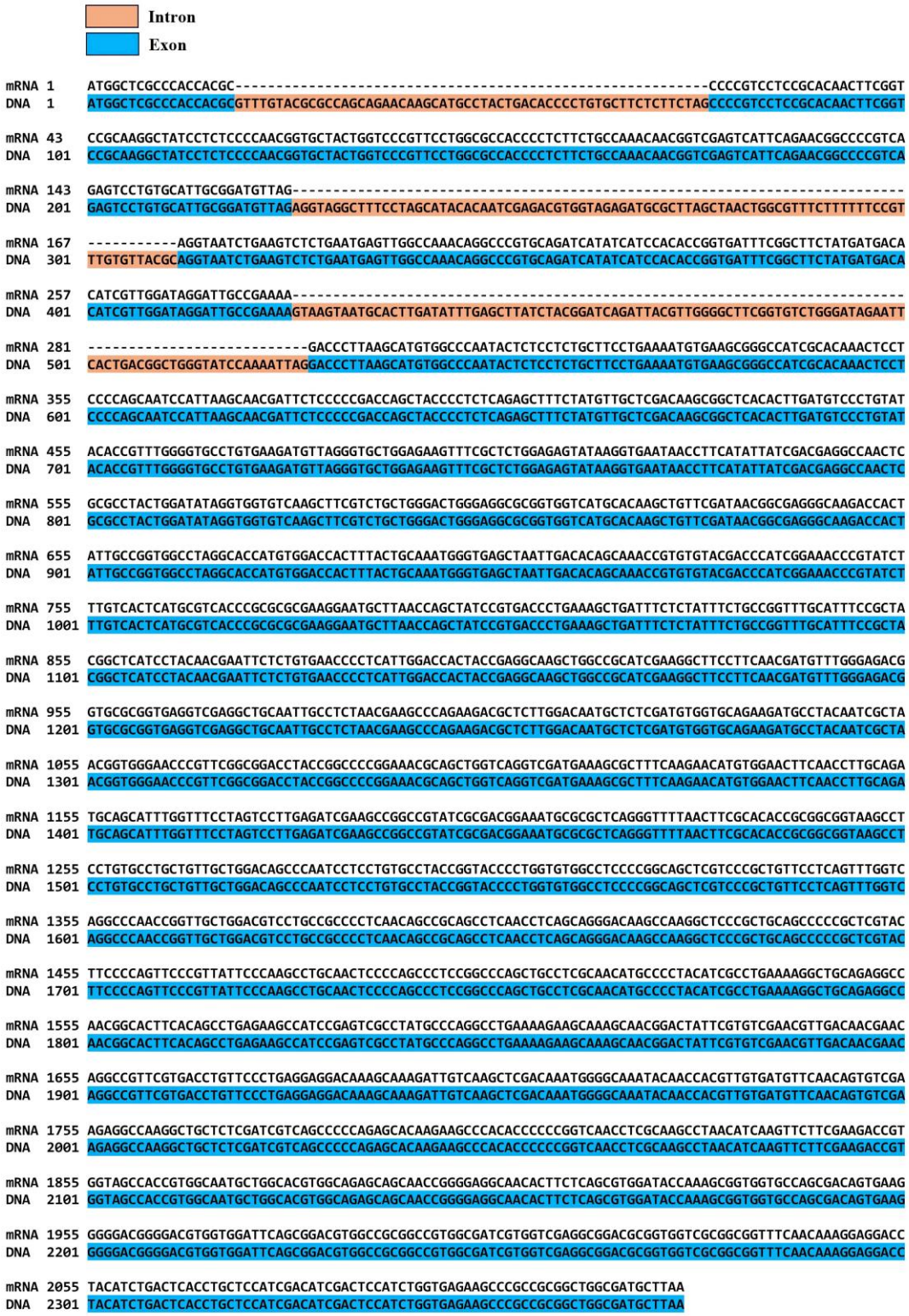

Supplementary Fig. 8. Nucleotide sequence and the intron and exon structure of the *ntp1* gene.

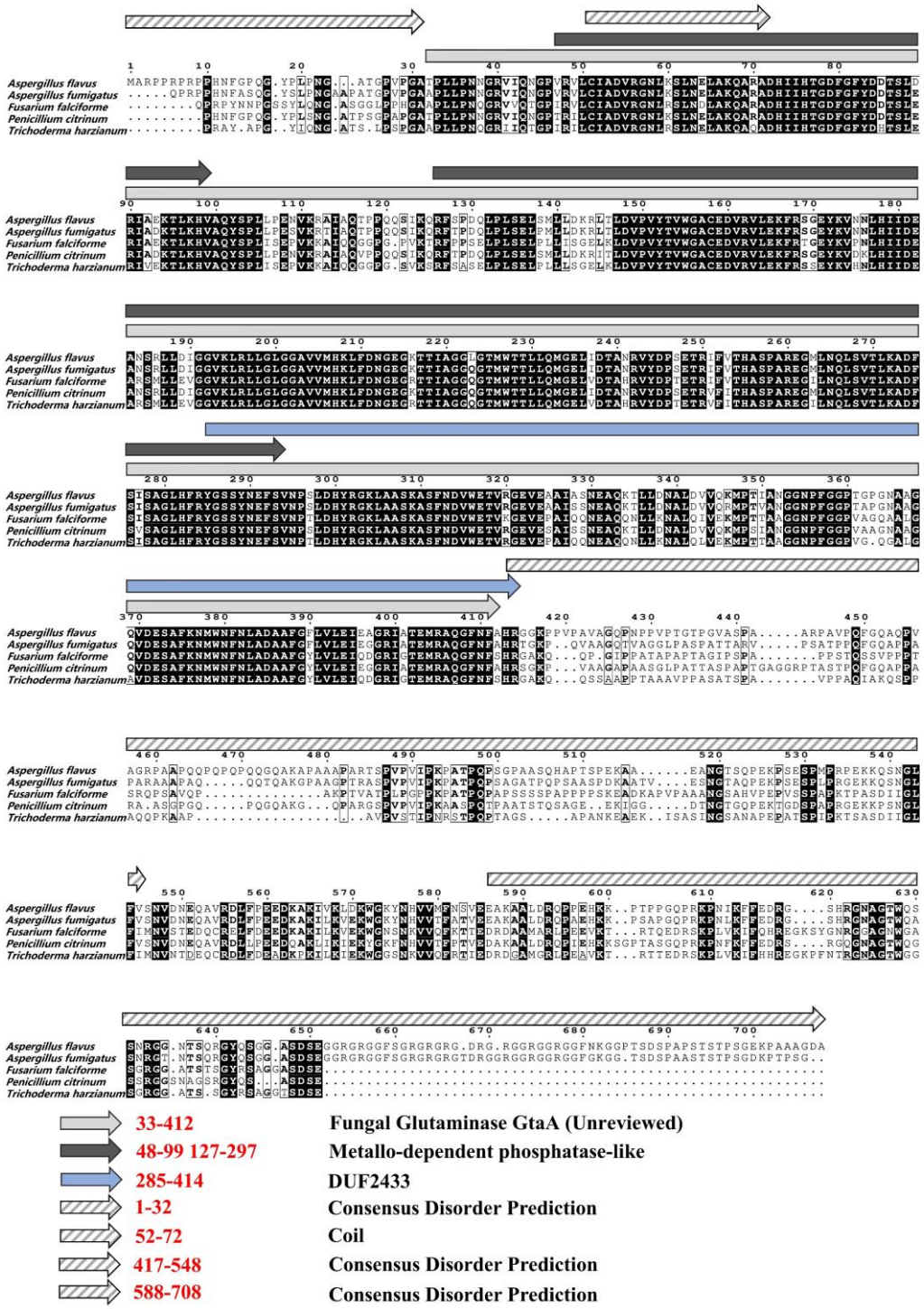

Supplementary Fig. 9. Multiple sequence alignment and domain characterization of Ntp1 proteins across diverse mycelial fungal species. The multiple sequence alignment encompassed Ntp1 proteins from five mycelial fungal species: *Aspergillus flavus*, *Aspergillus fumigatus*, *Fusarium falciforme*, *Penicillium citrinum*, and *Trichoderma harzianum*. Key motifs and protein domains, as identified via the Pfam database, are denoted in the alignment.

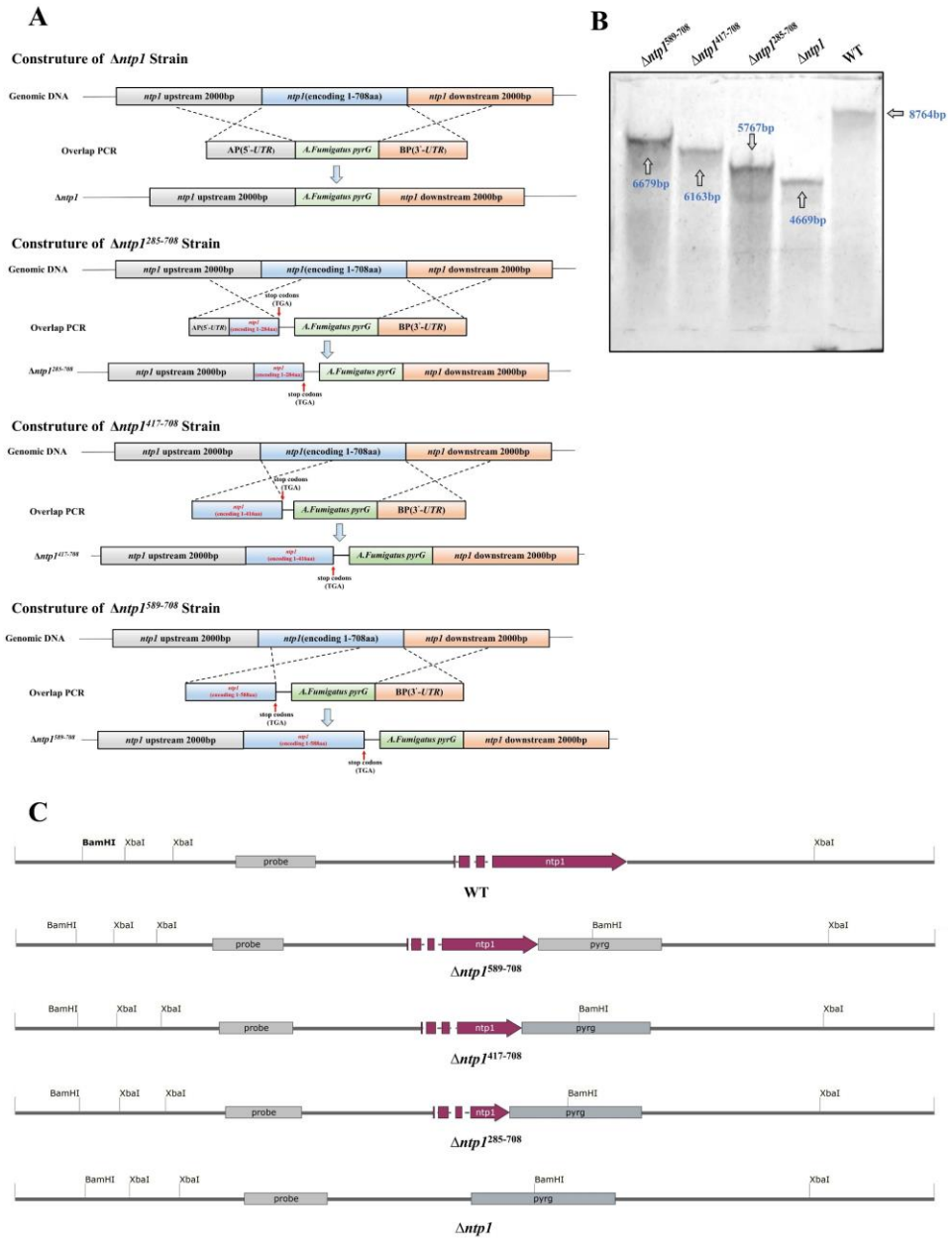

Supplementary Fig. 10. Gene replacement diagram and Southern blot analysis of WT and Npt1 truncated mutation strains. (**A**) Gene replacement diagram illustrates the process of constructing a deletion strain via homologous recombination. (**B**) Southern blot analysis of whole-cell DNA from various strains, digested with *BamHI* and *XbaI*, displaying unique band patterns that distinguished the WT strains from Ntp1 truncated mutation strains, detected using a DIG-labeled DNA probe on a nylon membrane. (**C**) Schematic representation of the Npt1 gene locus, detailing upstream and downstream regions. Key restriction sites are highlighted, with the grey box denoting the probe binding site. Restriction enzymes BamHI and XbaI are labeled to indicate their respective cleavage sites. Source data are provided as Source Data file.